MODELING OF INELASTIC BEHAVIOR OF RC STRUCTURES UNDER SEISMIC LOADS, ASCE LIBRARY, 2001, (ED) BENSON SHING AND TADA-AKI TANABE

2D and 3D Multi-directional Cracked Concrete Model under Reversed Cyclic Stresses

Koichi Maekawa[1], Naoyuki Fukuura[2] and Xuehui An[1]

Abstract

For predicting dynamic behavior of RC structures, in-plane spatially averaged constitutive models of RC elements with up to 4-way cracking are developed. The compression, tension and shear stress-strain relationships are applied on a couple of quasi-orthogonal cracks, using an active crack coordinate concept. Element based experiments of RC with multi-directional cracks are carried out for verification. By applying the in-plane models to orthogonally crossed sub-planes, the 2D models are extended to generic 3D models with multi-directional cracks. Experiments of 2D and 3D members and structures under reversed cyclic static and dynamic loads are simulated for both pre and post peak regions with the proposed analytical models.

Introduction

Performance based design needs a reliable system for predicting structural response and checking that safety, serviceability and durability performance objectives are achieved. With continuing development in both computer hardware and material research, nonlinear dynamic finite element analysis is a viable tool for simulation of laboratory experiments and performance assessment of RC structures. In order to model 3D structural geometries, stress states and loading patterns for RC structures subjected to non-proportional dynamic loading, many research efforts have addressed the development of advanced numerical methods including 3D constitutive modeling of reinforced concrete with multi-directional cracks.

[1] Department of Civil Engineering, The University of Tokyo, Hongo 7-3-1, Bunkyo-ku, Tokyo 113-8656, Japan

[2] Research Institute of Taisei Corporation, Nase-cho 344-1, Totsuka-ku, Yokohama 245, Japan

Previously, a quasi-orthogonal two-way cracking model was developed for analyzing wall-type RC structures under cyclic shear using a simplified active crack scheme (Okamura et al., 1991). However, this model is not appropriate for representing the behavior of 3D cases such as RC tanks (shell structure), RC short columns subjected to combined normal tension and cyclic shear and 3D RC structures under non-proportional loading paths (see Figure 1). For these systems, the number of crack orientation will reach 3 or 4. In Figure 1, two-way diagonal cracks and non-orthogonal flexural cracks can be identified.

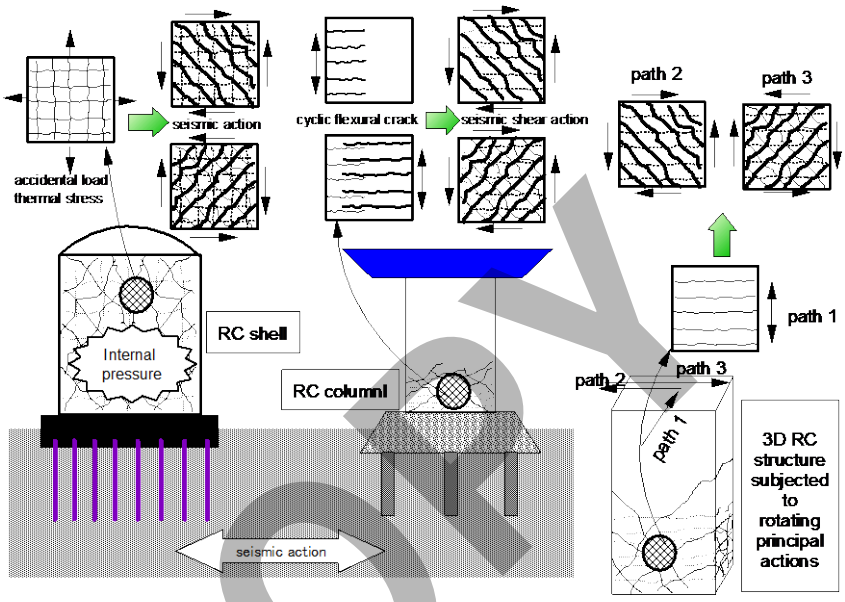

FIGURE 1. Multi-directional cracking of 3D RC structures under multi-directional loads

In order to represent 4-way cracks in RC structures, a multi-directional cracking system, with up to 4 independent orientations, is developed for the RC in-plane element. A fixed crack approach is used to facilitate computation. The shear transfer that causes principal stress rotation is included in the formulation by defining the normal and high strength concrete to have different crack surface roughness. After careful verification, the proposed in-plane nonlinear constitutive models are extended to 3D solid RC elements for practical usage.

Spatially averaged constitutive model of RC for finite element

In-plane active coordinate hypothesis

The basic assumption for dealing with multi-directional cracking in RC element is to ignore the interaction between the non-orthogonal cracks. The crack that exhibits the greatest non-linearity (the one with the largest cracking opening) is

selected as the active crack, and the concrete stress computation is carried out along it. The other cracks are considered to be dormant ones, and assumed to have less contribution to the non-linear stress-strain computation. The active crack approach is easy to use and has been applied successfully to the quasi-orthogonal two-way cracking model (Okamura et al., 1991). A similar concept is used for simulating the behavior of RC with 4-way cracking (Fukuura et al., 1998). Two orthogonal coordinates are applied to 4 cracking directions, with a couple of cracks in each of the coordinates. In this study, the couple of cracks can be quasi-orthogonal ones, satisfying the condition that the angle between these two cracks is larger than 67.5 degrees and less than 112.5 degrees. The active crack approach is applied to both couples of cracks. For each crack couple, one candidate of active crack is selected for stress computation. A single active crack is identified by comparing the non-linearity of the two candidate cracks.

When multi-directional cracks are introduced to an RC domain, overall non-linearity is generally dominated by one pair of cracks. Typically a second pair of cracks is not activated due to the comparatively higher stiffness owing to less crack width. Here, the active crack concept is used for choosing the active cracking coordinate. The coordinate having larger non-linearity is set as the active one, and the stresses computed in the dormant cracking coordinate are ignored. A flow chart shown in Figure 2 explains how to calculate stresses of an RC element with 4-way cracks. The stress of RC is composition of concrete stress and steel stress. In this model, the path-dependent behavior of RC is simulated by recording the path-dependent parameters in both of these two coordinates. As few path-dependent parameters of the basic RC constitutive model need to be recorded in computation, the memory size used in computation is acceptable.

Figure 2 shows how to apply orthogonal coordinate systems to a cracked RC element (Figure 2). By judging the calculated stress in a non-cracked RC element, the cracking condition can be identified. When the first crack occurs, the orientation of the 1st coordinate axes is established (A in Figure 2). **X**-axis of the 1st coordinate axes is defined parallel to the normal vector of the first crack. Then the computation follows the procedure for cracked concrete. After the second crack occurred, by evaluating the later stress condition based on the 1st coordinate axes, the orthogonal coordinate system may be adjusted, according to the angle between the 1st and 2nd cracks. If the angle between the 1st and 2nd cracks satisfy the quasi-orthogonal condition (within an angle between 67.5 degree and 112.5 degree), the 1st coordinate is kept for these quasi-orthogonal cracks (C in Figure 2). In this case, one of the two cracks has to be identified as an active crack for concrete stress computation. The crack with the larger tensile strain normal to the crack surface is chosen as the active crack, then the stress of concrete is computed on the basis of this crack. To provide a smooth switching of the “active crack” between these two coordinates, the switching happens when tensile strain of active crack is larger than 1.2 times the tensile strain of the dormant crack.

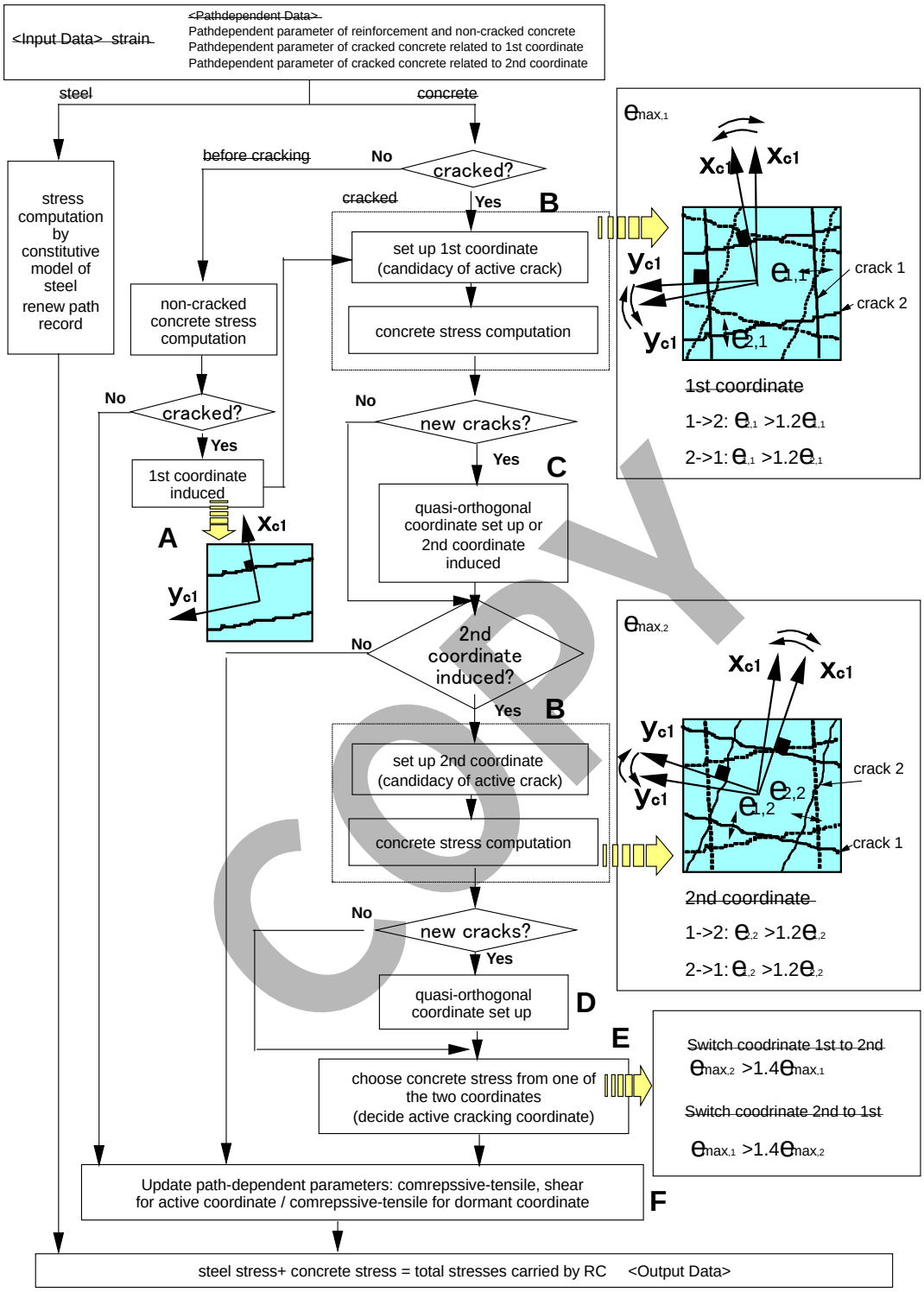

FIGURE 2. 4-way cracks and 2 quasi-orthogonal coordinate systems

If the angle between the 1st and 2nd cracks does not satisfy the quasi-orthogonal condition, the second orthogonal coordinate system is applied to

the second crack (C in Figure 2). The same procedure is used for the 3rd and 4th crack, as was used for the 2nd crack can be applied (D in Figure). Finally, two orthogonal coordinate systems are applied to the 4 cracks in different directions.

It is assumed that when a strain increment is applied to the RC domain, shear slip will occur in the active cracking coordinate of the quasi-orthogonal cracking system described above. The second coordinate system is considered dormant in shear, having no contribution to the non-linearity of RC element. The fixed 2-way smeared cracking model for reinforced concrete (Okamura et al., 1991) is extended to the quasi-orthogonal coordinate and applied on the couple of active cracks, then stress can be calculated for the RC domain with up to 4-way cracks. The switching between two coordinate systems is decided by the following criteria: the crack in the active cracking coordinate always has a larger normal strain (a larger crack opening).

The computation of concrete stress in an RC element with two quasi-orthogonal coordinates is summarized as following:

1) From each of the coordinate axes, a candidate active crack is selected from the two quasi-orthogonal cracks;

2) For each of the coordinates axes, the concrete stress is calculated on the basis of the identified candidate active crack;

3) Identify the active cracking coordinate axes by comparing the maximum tensile strain in each coordinate (safety factor of 1.4 is adopted to ensure a smooth switching);

4) Use the concrete stress of the active coordinate for RC stress computation.

The update of path-dependent parameters is carried out on both of the active and dormant coordinates. Only the shear transfer related path-dependent parameters are not updated for the dormant coordinate on which the plasticity of shear slip accumulates only if the crack is active (F in Figure 2).

An appropriate crack initiation criterion for previously cracked concrete is not known. In this study, the stress dependent cracking criteria for the un-cracked concrete are adopted.

Some numerical tests have been carried out for verification of interaction between quasi-orthogonal cracks (Fukuura et al., 1998). An example of these computational tests shows the behavior of RC with 3-way cracks (See Figure 3). During the first step, tensile loads are applied in X-Y directions to induce the 1st and 2nd cracks. In the second step, a diagonal crack is induced by shear loading. From the computational results, it is seen that the opening and shear slip along the 1st and 2nd crack enters an unloading path while the 3rd crack opens. According to the active crack approach, in step 1, the active couple of cracks are the 1st and 2nd cracks and

the 1st coordinate system (X-Y) is applied on these two cracks. In step 2, the active coordinate system switches into the direction of the 3rd crack and the X-Y coordinate changes into a dormant one.

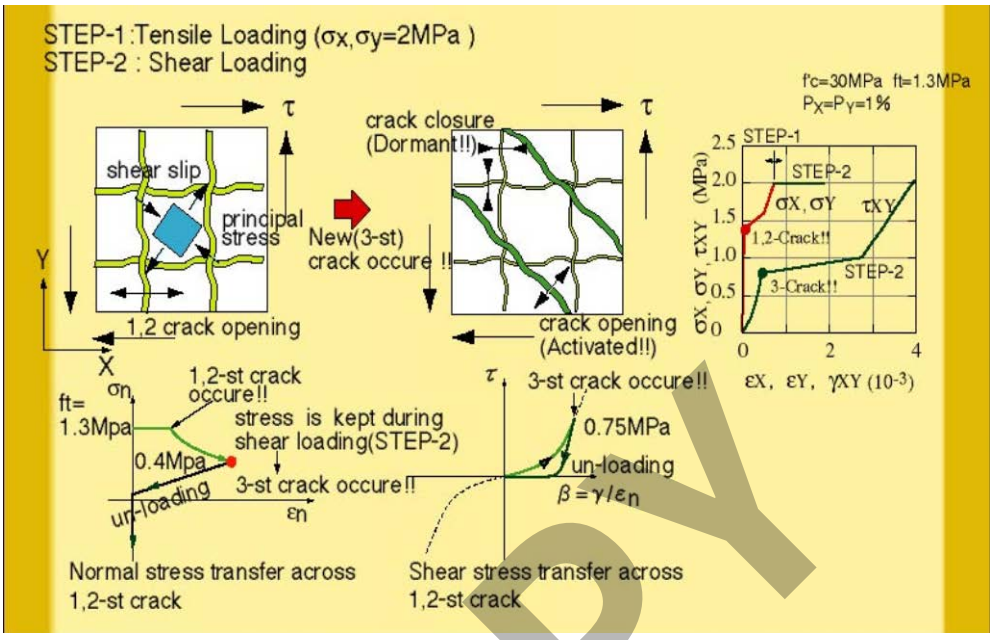

FIGURE 3. Numerical test example of quasi-orthogonal 3-way crack

Constitutive models in the active cracking coordinate

In an RC element, the average strain defined in the global coordinate system is converted to a local strain field defined in the active coordinate system. The stress transfer across the two active cracks is computed using the local constitutive models, including a coupled compression-tension model and a shear transfer model.

The normal stress transfer is provided by both continuum concrete in compression and bond accompanying stiffened tension through re-contact action. The coupled compression-tension model covers both the softening stress at crack planes of fracturing concrete and the tension-stiffening effect rooted in the bond stress transfer between cracks (Figure 4). Furthermore, the reduced performance of compressive stress transfer due to the orthogonal crack opening (Vecchio et al., 1986) is represented as additional damage by factorizing the axial coupled stress with ω, the fracture parameter reduction factor, as shown in Figure 4.

For computing the local shear stiffness on each crack, the contact density model for shear transfer (Li et al., 1989) is employed. In Figure 5, the transferred shear is assumed to be defined uniquely by the normalized shear strain. This removes the crack spacing as a parameter in the constitutive equations.

In the case of one-way cracking being induced in the RC element, the total

average shear strain is the composition of shear deformation due to both cracking and shear deformation of un-cracked concrete area. As shown in Figure 5a and 5b, the average shear stress is easy to calculate from the average shear strain and tensile strain normal to the crack surface. During cyclic loading, the stiffness at the cracking location increases rapidly as the crack is about to close. Thus, it is necessary to include the stiffness of un-cracked concrete in an RC element. Figure 5b shows a relation of shear transfer stress and normalized shear strain used in this study.

When two-way cracks are induced in one active coordinate system, the spatial average shear strain is defined by the shear slip along both cracks and deformation of the concrete continuum. Then the overall shear stiffness is computed by combining the secant shear stiffness of the two active cracks and the un-cracked concrete (See Figure 5c and 5d). As the path-dependent behavior of these two quasi-orthogonal cracks may be different, all of the possible loading-unloading-reloading combinations are considered and the separation of strains on different cracking surfaces is possible. The path-dependent parameters are the maximum shear strain (plus and minus) on both of the cracks.

An isotropic spatial average steel model

A spatially averaged stress-strain relationship for steel reinforcing bar is applied in the cracked RC domain (Figure 6a). This is accompanied by the tension-stiffening concrete model described in Figure 4. This bilinear steel model originally developed by Okamura et al. (1991), is modified to simulate the behavior of steel exhibiting large plastic deformations (Salem et al., 1999).

To incorporate the steel model in 2D in-plane analysis, the angle between the crack surface and the steel bar is used to determine the average yielding strength of steel (See Figure 6b). In order to have an efficient algorithm for cyclic analysis, a mutli-surface plasticity model is used for path-dependent computation (Figure 6c). This path-dependent approach has similar accuracy with Kato's model (Kato, 1979). However, in Kato's model, all the stress and strain history at the load-reversing point has to be stored in memory. In this proposed model, only 20 history variables including maximum strain, maximum plastic strain and each multi-plastic strain, are stored.

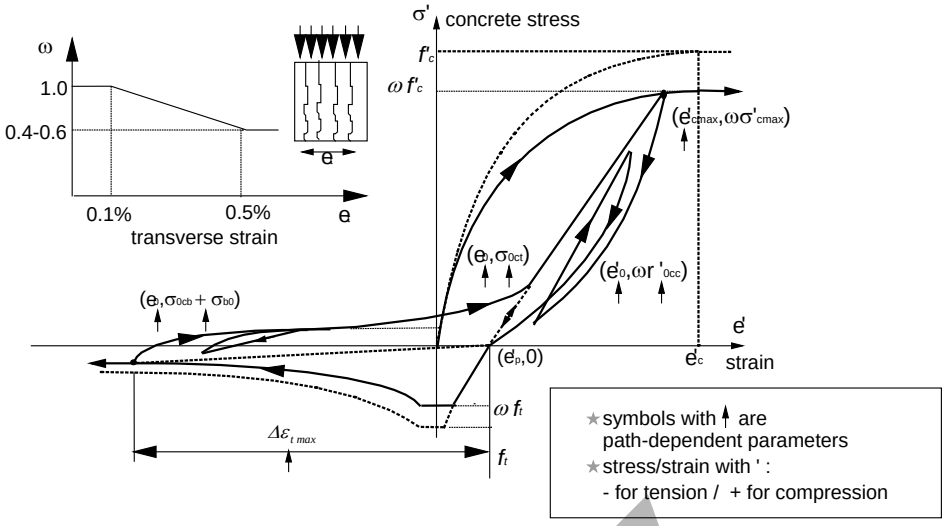

a) Coupled normal compressive and tensile stress

b) Compressive model

A) Loading : $\varepsilon \le \varepsilon_{c\,max}$

$$\sigma_{cc} = \omega K_0 E_{c0}(\varepsilon - \varepsilon_p)$$

$$E_{c0} = E_0 \frac{f_c}{\varepsilon_c}$$

B) Re-loading: $\varepsilon > \varepsilon_{c\,max} and \varepsilon \le \varepsilon_0$

$$\sigma_{cc} = \omega\left(\sigma_{c\,max} - (\sigma_{c\,max} - \sigma_{0cc}) \cdot \frac{(\varepsilon_{c\,max} - \varepsilon)}{(\varepsilon_{c\,max} - \varepsilon_0)}\right)$$

C) Unloading: $\varepsilon > \varepsilon_{c\,max} and \varepsilon > \varepsilon_0$

$$\sigma_{cc} = slop + \left(\frac{\sigma_{0cc}}{K_0 E_{c0}(\varepsilon_0 - \varepsilon_p)} - slop\right)\left(\frac{\varepsilon - \varepsilon_p}{\varepsilon_0 - \varepsilon_p}\right)^{PN}$$

ε_p : plastic strain $= \left(\frac{\varepsilon}{\varepsilon_c} - \frac{20}{7}\left(1 - e^{\left(-0.35\frac{\varepsilon}{\varepsilon_c}\right)}\right)\right) \cdot \varepsilon$

E_{c0} : initial stiffness

K_0 : fracture parameter $= e^{\left(-0.73\frac{\varepsilon}{\varepsilon_c}\left(1 - e^{\left(-1.25\frac{\varepsilon}{\varepsilon_c}\right)}\right)\right)}$

E_0 : fixed as 2.0

$\sigma_{c\,max}$: maximum compressive stress

$\varepsilon_{c\,max}$: maximum compressive strain

σ_{0cc} : current stress (before reducing)

ε_0 : current strain

ω : fracture parameter reducing factor

slop : unloading curve character, =2.0

PN : unloading curve character, =2.0

f_c : axial compressive strength, <0

ε_c :strain at axial compressive strength, <0

b) Tensile model

A) Loading : $\varepsilon \le \varepsilon_{c\,max}$

$$\sigma_{cb} = \omega f_t \left(\frac{\varepsilon_{tu}}{\varepsilon}\right)^c$$

B) Re-loading: $\varepsilon > \varepsilon_{c\,max} and \varepsilon \le \varepsilon_0$

$$\sigma_{cb} = \left(\sigma_{t\,max} - ((\sigma_{t\,max} - \sigma_{b0}) - \sigma_{0cb}) \cdot \frac{(\varepsilon_{t\,max} - \varepsilon)}{(\varepsilon_{t\,max} - \varepsilon_0)}\right) + \sigma_{b0}$$

$$\sigma_{b0} = -f_t\left(0.05 + 0.15\frac{\Delta\varepsilon_{t\,max}}{5\varepsilon_{tu}}\right) > -0.2\,f_t$$

C) Unloading: $\varepsilon > \varepsilon_{c\,max} and \varepsilon > \varepsilon_0$

$$\sigma_{cb} = E_{b0}(\varepsilon - \varepsilon_p) \cdot \alpha + \sigma_{b0} < R_f\, f_t$$

$$\alpha = slop + \left(\frac{\sigma_{0cb}}{E_{b0}(\varepsilon - \varepsilon_p)} - slop\right)\left(\frac{\varepsilon - \varepsilon_p}{\varepsilon_0 - \varepsilon_p}\right)^{PN}$$

$$E_{b0} = \frac{(\sigma_{t\,max} - \sigma_{b0})}{\Delta\varepsilon_{t\,max}}$$

ε_p : plastic strain by compression loading

σ_{b0} : residual stress by bond effect (<0)

$\Delta\varepsilon_{t\,max}$: maximum tensile strain

c : bond characteristic parameter

$\sigma_{t\,max}$: maximum tensile stress

$\varepsilon_{t\,max}$: maximum tensile strain

σ_{0cb} : current stress

ε_0 : current strain

ω : fracture parameter reducing factor

slop : unloading curve character, =0.0

PN : unloading curve character, =3.0

f_t : axial tensile strength, >0

ε_{tu} :cracking strain

FIGURE 4. Coupled normal compressive and tensile stress along and normal to cracks

$\tau = G \cdot \gamma$

τ : average shear stress

γ : average shear strain $\gamma = \gamma_c + \gamma_{cr}$

G : shear secant modulus of cracked concrete

$G = 1/(1/G_c + 1/G_{cr})$

G_c : Shear secant modulus of non-cracked concrete

G_{cr} : Shear secant modulus on the crack surface

$G_{cr} = \tau_{st}(\beta)/\gamma_{cr}$

$\tau_{st}(\beta)$: shear transfer stress on the crack surface

γ_{cr} : average shear strain due to the shear deformation of the crack

ε_t : average tensile strain normal to the crack

γ_c :average shear strain of the non-cracked concrete part

f_{st} :shear transfer strength on the crack surface

a) Average shear stress along one-way crack

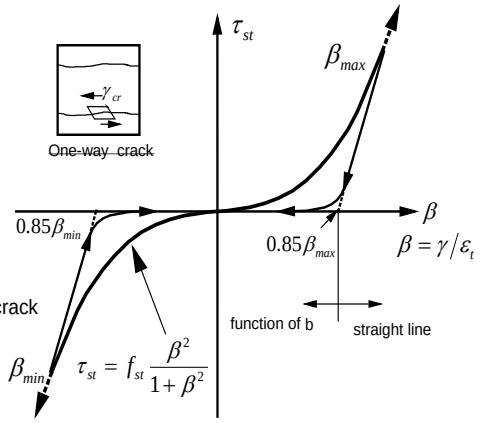

b) shear transfer model along one-way crack

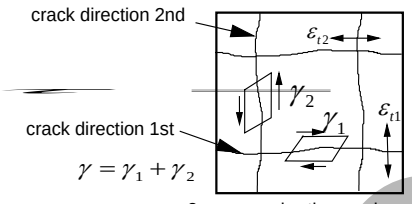

2-way quasi-orthogonal cracks

$\tau = G \cdot \gamma$

τ : average shear stress

$\tau = G_{cr1}\gamma_{cr1} = G_{cr2}\gamma_{cr2}$

γ : average shear strain $\gamma = \gamma_c + \gamma_{cr1} + \gamma_{cr2} \approx \gamma_{cr1} + \gamma_{cr2}$

$\gamma_c << \gamma_{cr1}, \gamma_{cr2}$

G : shear secant modulus of cracked concrete

$G = 1/(1/G_c + 1/G_{cr1} + 1/G_{cr2})$

G_c : Shear secant modulus of non-cracked concrete

G_{cr1} G_{cr2} : Shear secant modulus on the surface of crack No.1 and No.2

$G_{cr1} = \tau_{st}(\beta_1)/\gamma_{cr1}$ $G_{cr2} = \tau_{st}(\beta_2)/\gamma_{cr2}$

$\tau_{st}(\beta)$: shear transfer stress on the crack surface

γ_{cr1} γ_{cr2} : average shear strain due to the shear deformation of the crack

ε_{t1} ε_{t2} : average tensile strain normal to the crack

γ_c :average shear strain of the non-cracked concrete part

f_{st} :shear transfer strength on the crack surface

c) Average shear stress of concrete with two-way cracks

A) Loading at 1st and 2nd directions

B) Loading at 1st and unloading at 2nd direction

C) Unloading at 1st and 2nd directions

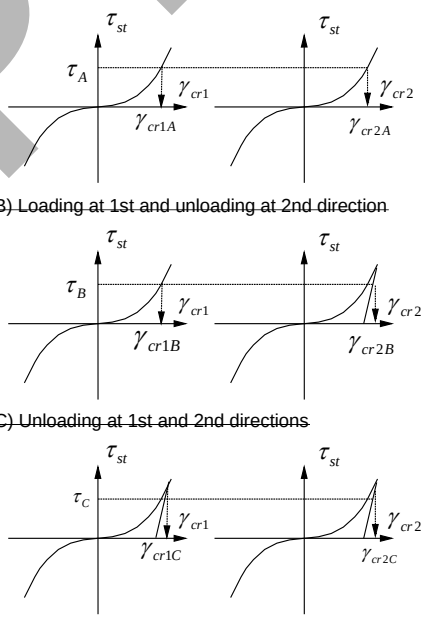

d) Shear stress path-dependent pattern on two cracks

FIGURE 5. Shear transfer along two-way cracks

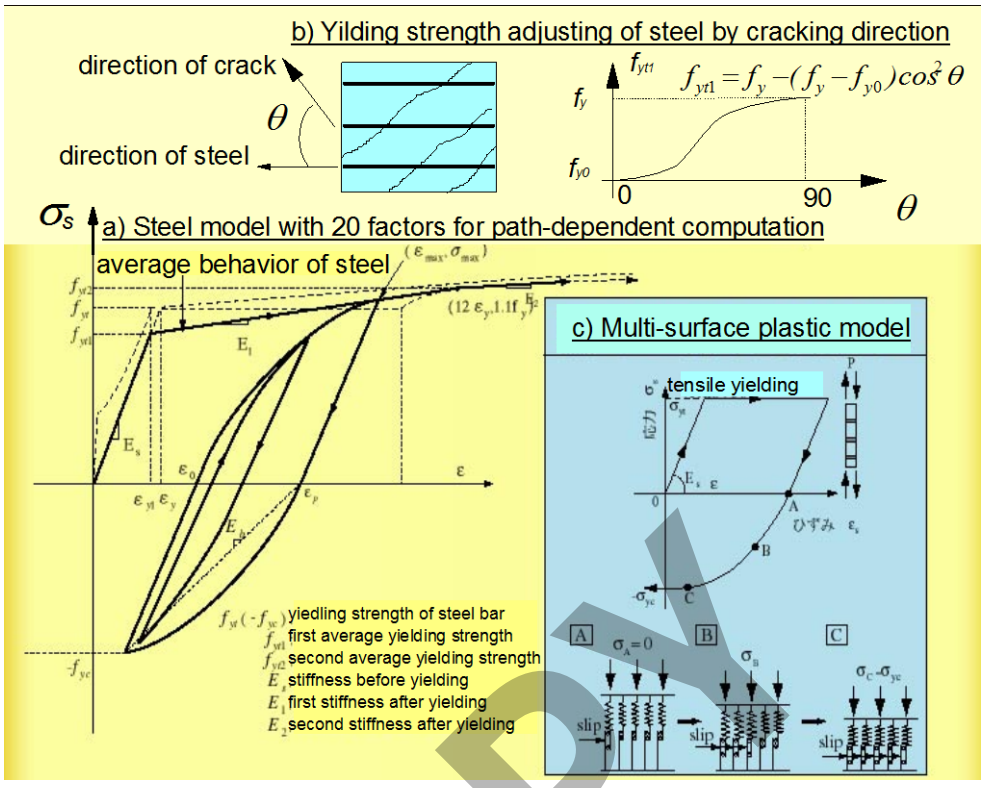

FIGURE 6. Spatially averaged stress-strain of steel in concrete

Extension of 2D-RC models to generic 3D

The multi-directional fixed smeared crack model is applied on a 2D plane RC element. In order to apply this in-plane model to 3D FEM analysis, a 3D orthogonal coordinate system is introduced with principal axis (1) normal to the initially introduced crack plane and the remaining axes (2 and 3) within the crack reference plane (Huake et al. 1998). This establishes three sub-spaces defined by axes (1,2), (2,3) and (1,3) in Figure 7. The in-plane cracked concrete models are employed within these subspaces. The initial crack is contained in (1,2) and (1,3) planes, while plane (2,3) is orthogonal to the plane of the initial crack. Additional cracking is represented on the basis of the fixed two-dimensional sub-spaces.The partial stresses defined by the crack projection on (i, j) can be computed using the in-plane RC constitutive law. The compressive strength of 3D cracked concrete solids is defined by extending the 2D compression field theory (Vecchio et al., 1986).

Element based verification

The basic constitutive models, such as the tension stiffening model, the elastic-plastic compression model and the shear transfer model, have been verified for the case of a single-directional crack using one dimensional experiments

(Okamura et al., 1991). However, in the case of the 2D in-plane model, the combination of these models needs to be verified for systems with multiple cracks. Here, element-based experiments are used as verification for an RC element with 2 to 4 directional cracks.

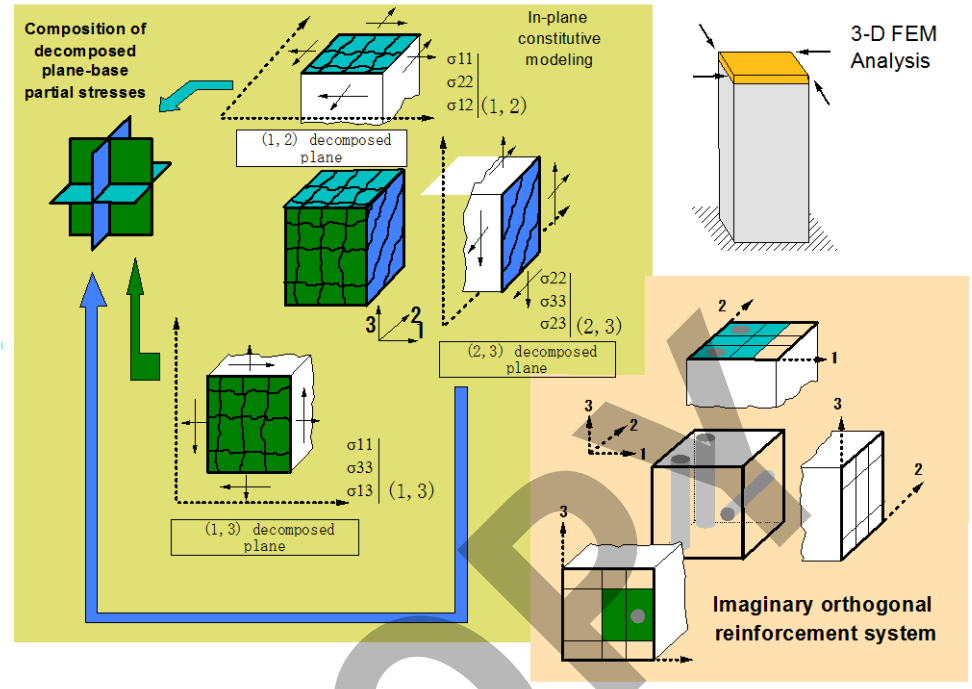

FIGURE 7. Breakdown and re-composition of load carrying mechanism of 3D cracked concrete

Verification of RC domain with up to 2-way cracks by RC panel experiments

The proposed constitutive model is verified through comparison of simulated and observed response for a series of experiments conducted on orthogonally reinforced panels subjected to monotonic and cyclic loading. The experiment series of RC panels subjected to monotonic load (Collins et al., 1982) are used to verify separately the tension, compression and shear transfer model of the concrete constitutive model, and the spatial average model of steel. The results of experimental testing of RC panels under cyclic shear loads are used to verify the combination of these constitutive models. Figure 8 shows simulated and observed response for three RC panels under cyclic shear loads. Parameters used to model these panels are shown in Table 1.

The response of three isotropically reinforced concrete panels subjected to reversed cyclic shear is shown in Figure 8. For panel SR10 (Figure 8a, Ohmori et al., 1989), since the reinforcement ratios in both directions are the same and the angle between induced crack and reinforcement in both directions does not differ, shear

transfer is not substantial. Simulated and observed response are compared for high levels of inelastic deformation in the concrete and steel. Cyclic tensile- compressive concrete response and steel hysteretic response are activated by this test.

Table 1 Experiments of RC panel under cyclic loads

Specimen	Reinforcement				Concrete		[2]Load condition	[3]Failure mode	Reference
	p_x (%)	f_{yx} (MPa)	p_y (%)	f_{yy} (MPa)	f'_c (MPa)	[1]f_t (MPa)	$\tau : F_x : F_y$		
SR10	1.02	398	1.02	398	36.5	1.96	1:0:0	Y	Ohmori et al., 1989
SP1.7	1.75	440	1.75	440	20.9	1.96	1:0:0	C	Yoshikawa et al., 1982
SE10	2.93	492	0.98	479	34.0	2.20	3:1:1	Y,C	Stevens et al., 1986

[1] Tensile strength of concrete used in analysis;

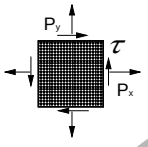

[2] As shown in this figure:

[3] Y: steel yielding; C: concrete failure.

The specimen SP1.7 shown in Figure 8b, is also an isoptropic RC panel loaded in pure shear (Yoshikawa et al., 1982). Here heavy reinforcement results in diagonal compression failure of cracked concrete with no yielding of steel. The results of this test enable examination of the concrete compressive model. The model leads to a higher capacity, but fair agreement is seen for the cyclic shear loop.

An anisotropically reinforced concrete panel (strong axis 3% and weak 1%) subjected to combined in-plane compression and cyclic shear is shown in Figure 8c. The panel SE10 by Stevens et al. (1986) failed in diagonal compression after yielding of weak axial reinforcement. Here the anisotropic arrangement of steel results in shear stress transfer across a crack. Since the load level at which steel yields is affected by the presence of transferred shear stress, SE10 is useful for checking the shear transfer model. It is shown that the capacity and hysteretic energy can be predicted with sufficient accuracy, except for the final loop with the largest strain. The prediction of internal hysteresis loops is related directly to the energy absorption capacity of RC structure and is important for dynamic analysis. For further improvement of modeling range, spalling of cover concrete and cyclic deterioration of material properties is needed.

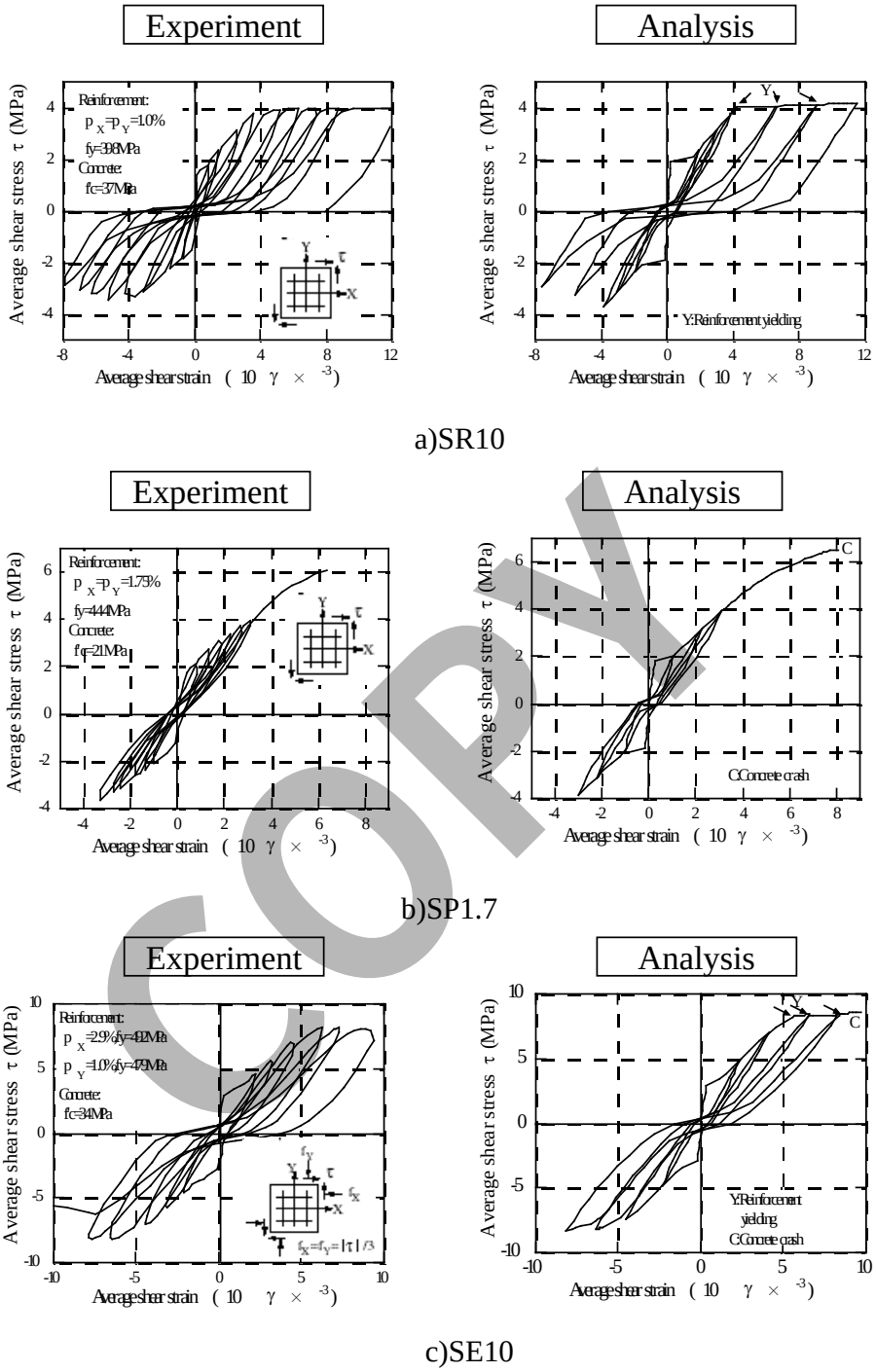

FIGURE 8. RC panel element under cyclic shear force

Verification of RC domain with multi-directional cracking

In order to verify the proposed multi-directional model for representing RC solids with up to 4-way cracks, several cylindrical test specimens were loaded under

axial tension, internal hydraulic pressure and reversed cyclic torsion (See Figure 9a, Fukuura et al., 1998).

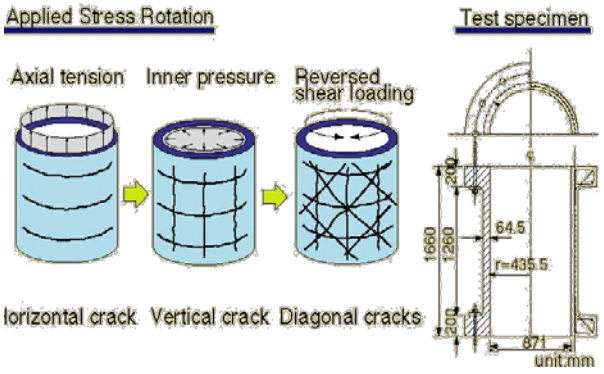

FIGURE 9a. Layout of experiment for multi-directional cracked RC

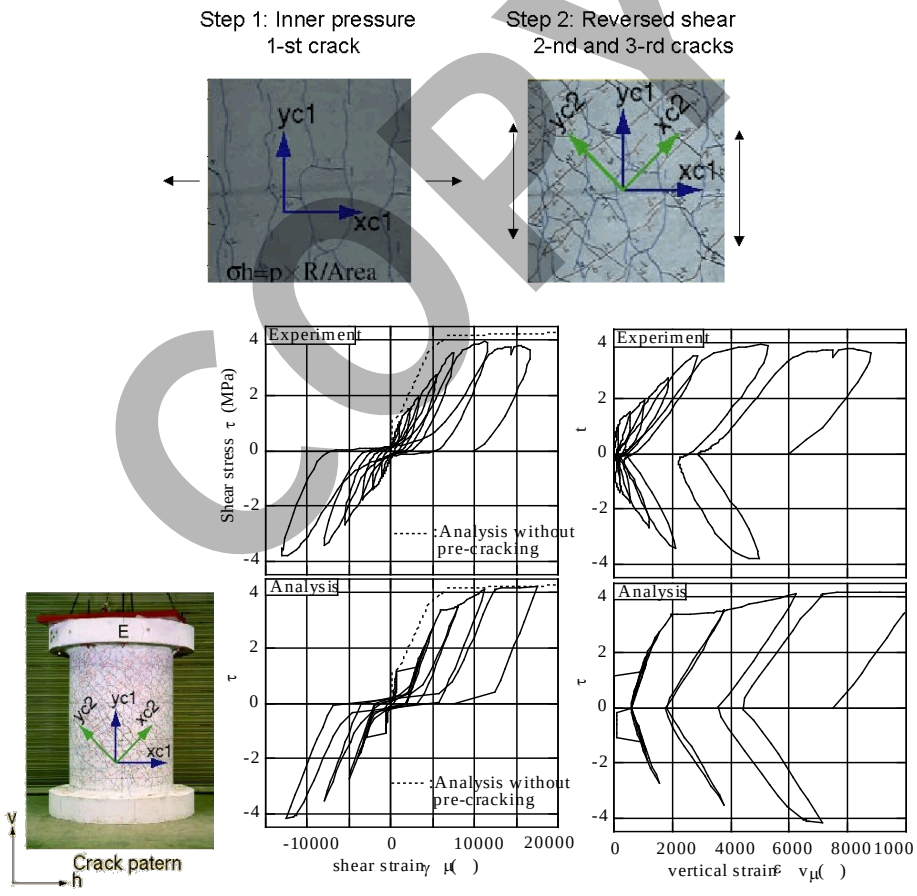

FIGURE 9b. Experimental and analytical behavior of specimen C-1 (3-way cracks)

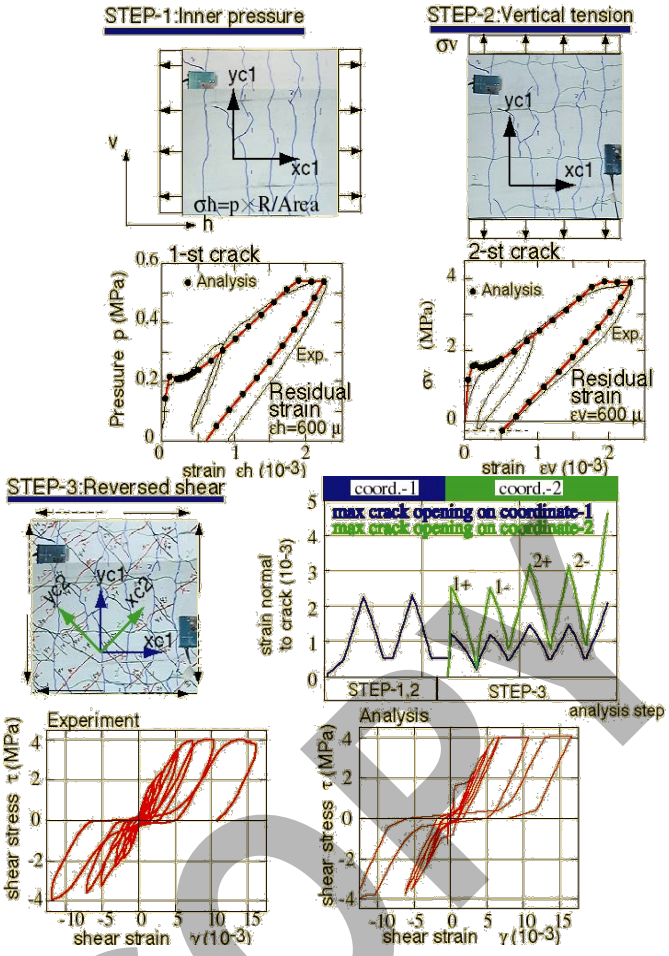

FIGURE 9c. Experimental and analytical behavior of specimen A-2 (4-way cracks)

For specimen C1, uniaxial tension is applied first to induce on-way cracking (Figure 9b). This results in large plastic deformation normal to the initial crack plane. Next, cyclic shear is applied, resulting in the development of new bi-directional shear cracks in addition to initial cracks. For specimen A-2, the internal pressure and axial action induce a pair of initial cracks, then the cyclic shear loads produce another couple of cracks, making the total number of fixed crack surfaces reach four (Figure 9c).

In the analysis, the initially induced cracks are represented by one coordinate axis and the diagonal shear cracks in the remaining two directions are treated as a pair with other coordinates. The normal tension and cyclic shear stress-strain behavior of these specimens is simulated fairly well by the proposed model (Figure 9b,c). Additionally the cracking behavior of each loading step is simulated well by the proposed model.

Member and structure based verification

RC shear wall under cyclic load

RC shear walls subjected to in-plane load are suitable for verification of nonlinear FEM analysis (Okamura et al., 1991). The nonlinear FEM program used in this study can predict the post-peak softening behavior of RC shear walls, as the strain softening behavior is represented in the proposed compressive model and the deformation localization behavior can be modeled using interface elements. Modeling this behavior is important for seismic performance evaluation of RC structures. Figure 10 shows the ductility analysis of one RC shear wall with multi-directional cracks (JCI, 1983) using the active smeared crack model. It can be observed that the analytical post peak behaviors are different between case 1 (without joint element at the bottom of RC wall) and case 2 (with joint element), but less difference is evident for maximum capacity. Joint element is useful for simulating the localized shear slip and pullout of steel from footing. It is found that when strain softening occurs in the wall the effects of bar pull-out and localized deformation at the construction joint must be included in an analytical model to accurately represent observed response.

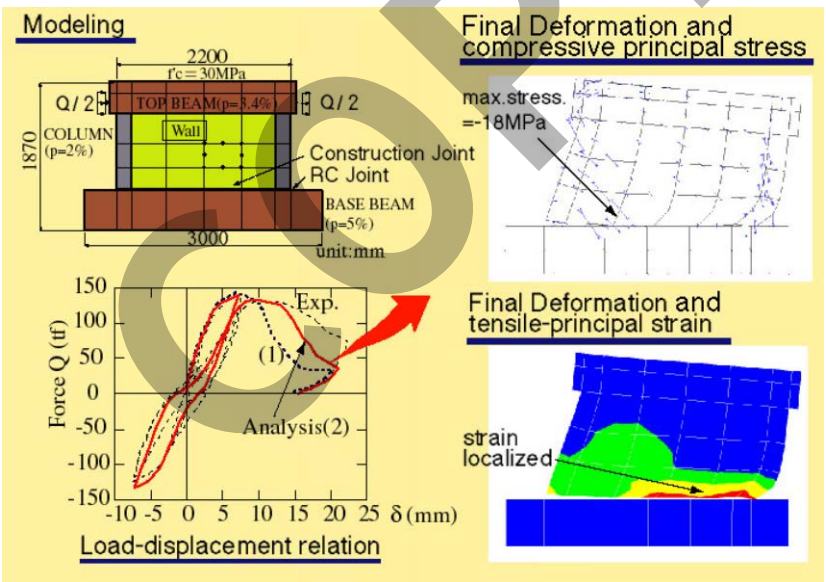

FIGURE 10. Deformation performance of RC wall under in-plane cyclic load

RC hyperbolic shell structure

Figure 11 shows a model experiment for a large cooling tower with cyclic loading applied to the top (Ouchi et al., 1977). Here response is simulated by FEM computation using 3D shell elements. Good agreement is found between the experimental and computational load-deformation results (Figure 10).

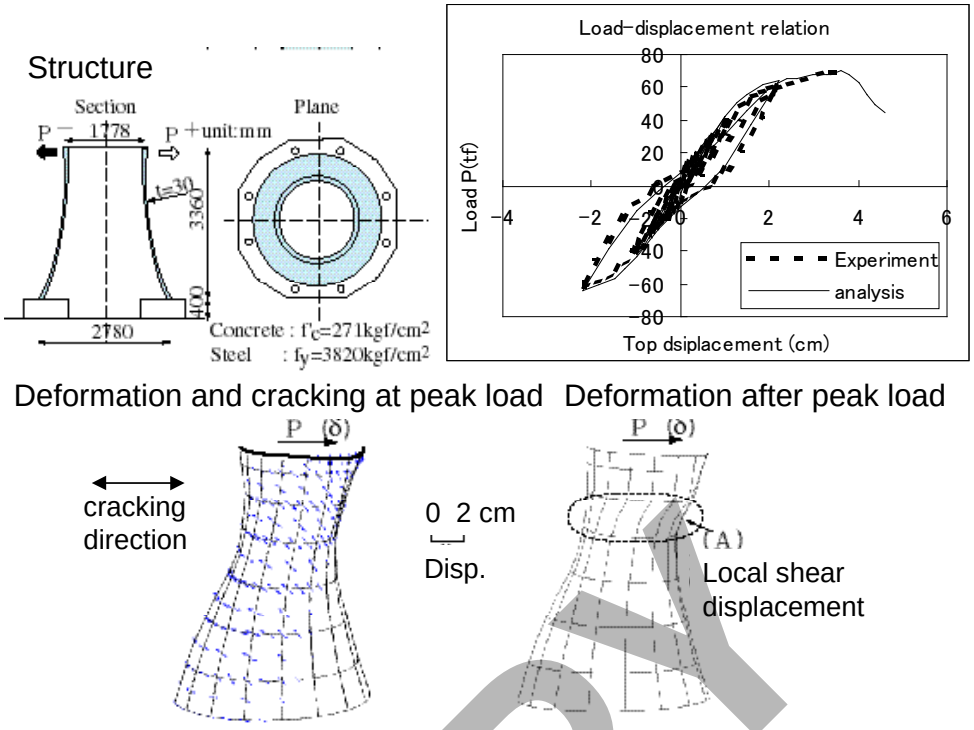

FIGURE 11. Analytical results of RC hyperbolic shell structure under cyclic load

The final failure observed in the experiment, is a sudden occurrence of shear collapse with obvious diagonal cracks close to the neck of the shell. The same deformational behavior can be identified in the computational results (See A zone in Figure 11). In this analysis, if the reduction of compressive strength due to the opening of orthogonal crack were not taken into account, the load decrease after peak (see Figure 10) would not happen.

Box type hollow section RC column under cyclic torsion, shear and bending load

3D FEM analysis was conducted to verify application of the proposed model for simulating the behavior of RC columns. Figure 12 shows simulated and observed response for a box-type hollow section RC column under cyclic torsion, shear and bending load (Masukawa et al., 1999). 3D RC shell elements are used in the analysis. The computed bending moment-curvature and torque-twist relationships are compared with the experimental data (Figure 12). The computational tool can predict effectively the deformation and stiffness under shear and bending. However for torsional loading, the simulated post-cracking stiffness and ultimate capacity are considerably higher than the experimental results. This is likely due to the fact that the proposed model doesn't represent observed cover concrete spalling under torsional loading. This reduction in torsion resistance caused by spalling will be addressed in a future model.

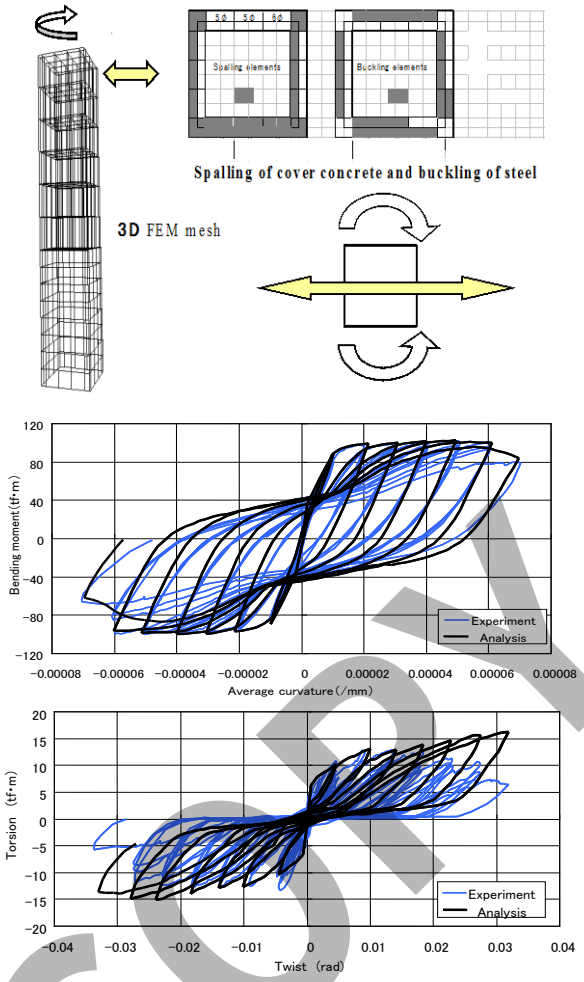

FIGURE 12. 3D analysis of hollow RC column under cyclic torsion, shear and bending load

RC 3D thin shell structure subjected to hydrostatic pressure with geometrical non-linearity

RC domes are used to cap underground LNG tanks. The load on the roof is caused by the covering soil. The dome structure is designed as a shell to carry the compressive load. Sudden collapse of the dome may occur if there is compression failure and spalling of the dome concrete. A 1/20 scale model of a dome was tested in the laboratory to verify the safety of the RC dome roof (Okamoto et al., submitted). The model dome was fixed up side down on a pressure tank. Here the water in the tank represents the hydrostatic pressure load (see Figure 13). The analytical model for this experiment is 1/4 of the model dome and uses 3D shell elements. Both material and geometric non-linearity are included in the numerical analysis. The comparison of computational and experimental results is shown in Figure 13. It can be concluded that material and geometric non-linearity is required to simulate the response of this dome structure.

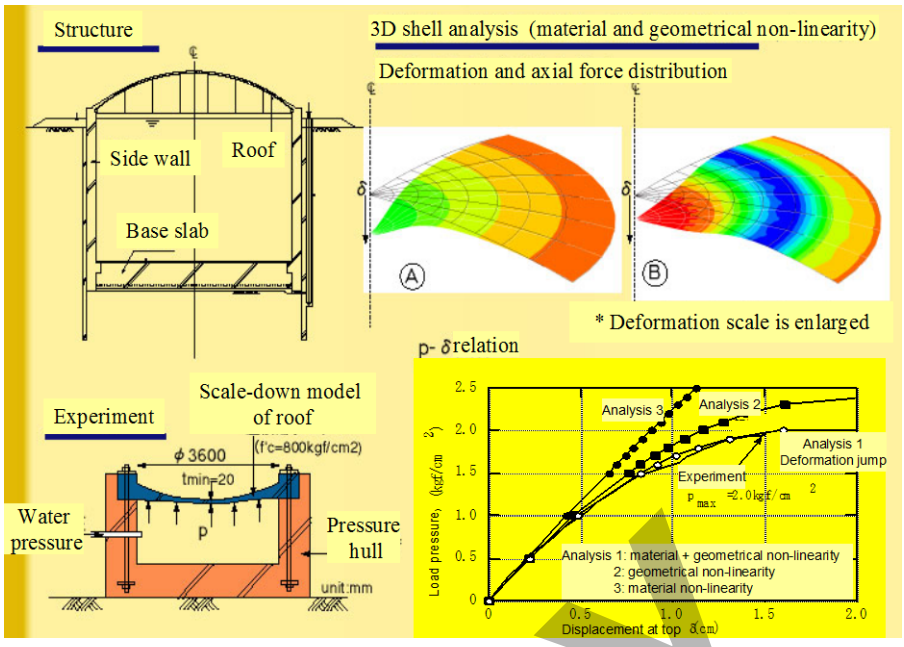

FIGURE 13. Analytical simulation of RC 3D thin shell structure

The observed large non-linear deformation is simulated well by the proposed model. Additionally the deformation patterns and the failure location show good agreement with experimental observation.

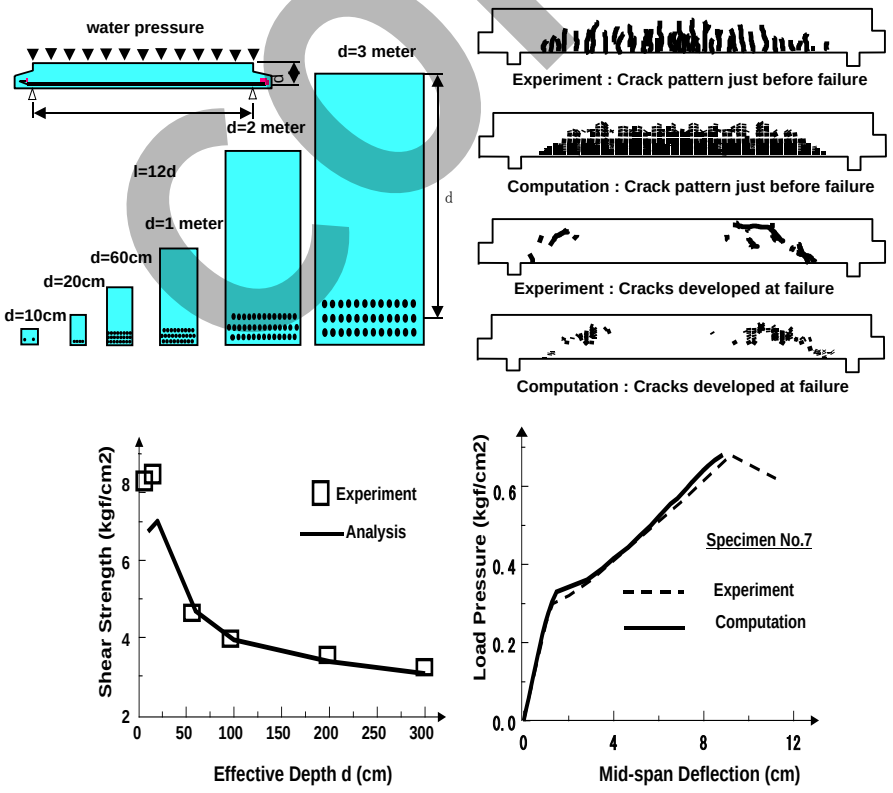

FIGURE 14. Computational results for size effect experiment

Shear failure and size effect of large RC beams without web reinforcement

In order to verify application of the model for simulating the response of large-scale RC structures, the ability of the model to simulate shear failure and size effect is evaluated by analyzing a series of experiments for beams, with depths varying from 10cm to 300cm (An et al., 1997). The results of this study are summarized in Figure 14. Shear behavior is predicted effectively for even the largest beam, including the shear capacity, shear stiffness and shear cracking process. The sudden diagonal shear crack, that was observed during the lab test, is predicted in the final computational step in the analysis.

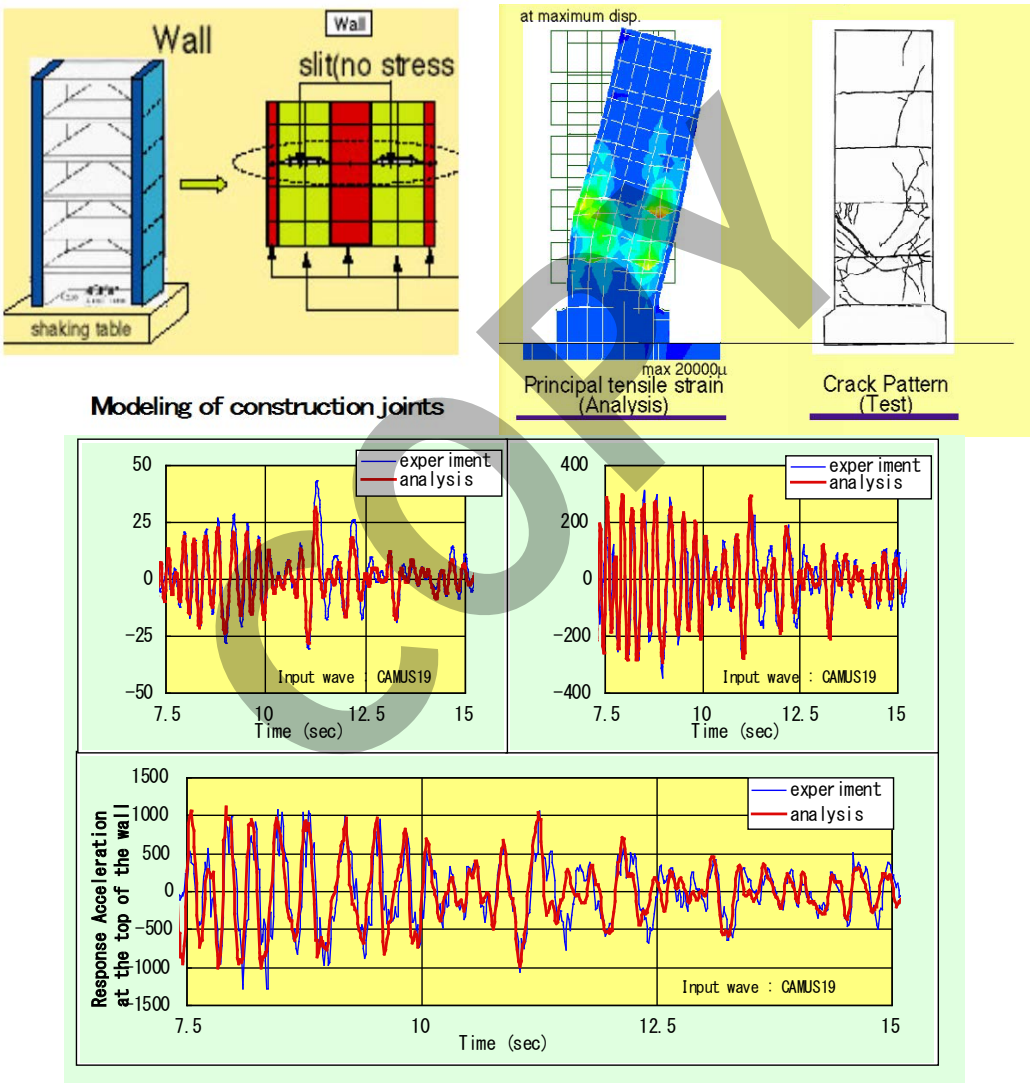

FIGURE 15. Benchmark dynamic analysis of shear wall (CAMUS, 1998)

RC 2D shear wall in dynamics

The nonlinear dynamic FEM code introduced in this paper has participated in an international benchmark dynamic analysis of multi-story shear wall (CAMUS project) in Paris in September 1998. In this benchmark analysis only the characteristics of the specimen, shaking table and the input acceleration were reported to the analyzers in advance. The experimental results were kept secret until all the analyses were presented. In Figure 15 (CAMUS, 1998) a comparison of simulated and observed responses is presented. The shear wall structure includes a large zone of plain concrete and in-plane shear failure controls wall response. Comparison of predicted and observed responses shows that the proposed model represents well the observed acceleration and displacement, the cracking pattern and final failure location for the system.

Conclusion and prospect

The proposed model is used within a dynamic nonlinear FEM program to simulate the behavior of RC structures with multi-directional cracks. A constitutive model for RC and plain concrete, based on the multi-directional crack concept, is introduced. Numerical simulation of laboratory experiments of RC systems subjected to cyclic loading is carried out for verification. The results from the international benchmark dynamic analysis of a multi-story shear wall are reported. Comparison of simulated and observed response at the member and structure level, indicates that the FEM tool is appropriate for seismic performance evaluation of RC structures. This research supports state-of-the art advancement in 3D modeling of RC structures.

The analytical results suggest that modeling the spalling of cover concrete and buckling of main reinforcing bars is of importance for predicting deformation capacity of some RC structures. Future research will focus on including these response models in 3D solid element to enable precise simulation of post-peak behavior, especially for small section flexural members.

References

An, X., Maekawa, K. and Okamura, H. (1997) “Numerical simulation of size effect in shear strength of RC beams,” *Journal of Materials, Concrete Structures and Pavements, JSCE*, Vol. 35, 297-316.

Commissariat a l'Energie Atomique (1998) “*CAMUS International Benchmark - Experimental results synthesis of the participants' report,” CEA and GEO, a French research network,* part of the CAMUS Working Group under the auspices of the French Association of Earthquake Engineering (AFPS).

Collins, M.P. and Veccho, F.J. (1982) *The response of reinforced concrete to in-plane shear and normal stress*, University of Tronoto, March.

Fukuura, N. and Maekawa, K. (1998) "Multi-directional crack model for in-plane reinforced concrete under reversed cyclic actions- 4 way fixed crack formulation and verification," *Computational Modeling of Concrete Structures, Euro-C,* 143-152.

Hauke, B. and Maekawa, K. (1998) "Three-dimensional R/C model with multi-directional cracking," *Computational Modeling of Concrete Structures, Euro-C,* 93-102.

JCI Shear Committee (1983), *Collected experimental data of specimens for verification of analytical models, JCI-C6,* October.

Kato, B. (1979) "Mechanical properties of steel under load cycles idealizing seismic action," *CEB Bulletin D'Information,* No.131, 7-27.

Li, B., Maekawa, K. and Okamura, H. (1989) "Contact density model for stress tranfer across cracks in concrete," *Journal of the Faculty of Engineering, University of Tokyo (B),* Vol.40, No.1, 9-52.

Masukawa, J., Suda, K. and Maekawa, K. (1999) "3-dimensional nonlinear FEM analysis of hollow bridge piers considering spalling of concrete cover and buckling of reinforcing bars," *Proceedings of the Japan Concrete Institute,* Vol. 21, No.3, 37-42.

Ohmori, N., Takahashi, T., Inoue, H., Kurihara, K. and Watanabe, S. (1989) "Experimental studies on nonlinear behaviors of reinforced concrete panels ubjected to cyclic in-plane shear," *Tran. AIJ*. 403, 105-118

Okamoto, T., Minegishi, K., Kuroda, M. and Watanabe, M. (Submitted) "Stability study of for concrete dome structure," *Journal of Materials, Concrete Structures, Pavements, JSCE.*

Okamura, H. and Maekawa, K. (1991) *Nonlinear Analysis and Constitutive Models of Reinforced Concrete*, Gihodo-Shuppan, Tokyo, Japan.

Ouchi, H., Koike, K., Ito, M. nad Takeda, T. (1977) "Experimental and analytical study on inelastic behavior of the RC cooling tower model subjected to horizontal loads," *Proceeding of JSCE,* No.266, October, 39-50.

Salem, H. and Maekawa, K. (1999) "Spatially averaged tensile mechanics for cracked concrete and reinforcement under highly inelastic range," *Journal of Materials, Concrete Structures, Pavements, JSCE*, Februrary, 277-293.

Stevens, N. J., Uzumeri, S. M. and Collins, M. P. (1986) *Analytical modeling of reinforced concrete subjected to monotonic and reversed loadings*, University of Toronto.

Vecchio, F. and Collins, M.P. (1986) "The modified compression field theory for reinforced concrete elements subjected to shear," *ACI Journal*, 3-4, 219-231.

Yoshikawa, H., Iida, H., Sumi, T., Nakagawa, A. and Yamagata, H. (1982) "Study on the shear behavior of reinforced concrete cylinders subjected to torsional loading," *Tech. Report of Hazama-gumi.*